Transition to chaos in converging–diverging channel flows: Ruelle–Takens–Newhouse scenario

A. M. Guzmán and C. H. Amon
Department of Mechanical Engineering, Carnegie Mellon University, Pittsburgh, Pennsylvania 15213

(Received 8 June 1993; accepted 7 February 1994)

Direct numerical simulations of the transition process from laminar to chaotic flow in converging–diverging channels are presented. The chaotic flow regime is reached after a sequence of successive supercritical Hopf bifurcations to periodic, quasiperiodic, and chaotic self-sustained flow regimes. The numerical experiments reveal three distinct bifurcations as the Reynolds number is increased, each adding a new fundamental frequency to the velocity spectrum. In addition, frequency-locked periodic solutions with independent but synchronized periodic functions are obtained. A scenario similar to the Ruelle–Takens–Newhouse scenario of the onset of chaos is verified in this forced convective open system flow. The results are illustrated for different Reynolds numbers using time-velocity histories, Fourier power spectra, and phase space trajectories. The global structure of the self-sustained oscillatory flow for a periodic regime is also discussed.

I. INTRODUCTION

The process by which a laminar viscous flow undergoes transition to turbulence through diverse routes is of fundamental fluid-dynamical interest. In closed system flows like Rayleigh–Bénard convection[1–3] and Taylor–Couette flow,[4,5] a sequence of ordered transitions may be discerned. As the control parameter is varied, the flow may become chaotic after three incommensurate bifurcations (Ruelle–Takens–Newhouse scenario[6,7]), after an infinite sequence of period-doubling bifurcations (Feigenbaum scenario[8]), or after an intermittency regime (Manneville and Pomeau scenario[9]). The choice of the transition scenario seems to be dependent on geometry, initial conditions, and other specific flow features.[3]

The stability of an equilibrium state can change either when an eigenvalue of its linearized behavior passes through zero, or a pair of nonzero eigenvalues crosses the imaginary axis.[10] The latter, called the Hopf bifurcation, involves a family of periodic orbits that grows from the equilibrium. The stability of periodic orbits can be studied by defining a Poincaré map by successive intersections of trajectories with a cross section of the periodic orbit.[11] Complex eigenvalues of modulus one are associated with the emergence of two-dimensional invariant tori in a flow. The dynamics on these tori involve a complicated succession of quasiperiodic solutions, whose power spectra have two incommensurate frequencies and phase-locked periodic solutions, which involve subharmonics of the original periodic solution.[10] The most explicit predictions made by Ruelle and Takens involve the number of bifurcations a flow undergoes in the transition from steady to aperiodic flow. Ruelle and Takens[6] investigated the structural instability of a quasiperiodic flow on a torus of dimension equal or greater than 2 and demonstrated that a quasiperiodic flow should not be observed. Later, Newhouse *et al.*[7] proved that a quasiperiodic flow on a three-dimensional torus could be perturbed to a flow with a structurally stable strange attractor. Then, according to the Ruelle–Takens–Newhouse theory,[6,7] the power spectrum of a dynamical system evolves as a function of the control parameter and consists of one frequency, then two and sometimes three frequencies. As soon as the third frequency arrives, the broadband noise characteristic of chaos should start to appear.

The two closed systems that have been most extensively studied experimentally in the context of transition to chaos and turbulence are Taylor–Couette flow and Rayleigh–Bénard convection.[11] The classical experiment of Gollub and Swinney,[4] using spectral analysis of laser-Doppler velocimetry measurements on Taylor–Couette flow, provided a remarkable verification of the Ruelle–Takens–Newhouse predictions. They clearly observed a transition between a quasiperiodic flow with two frequencies and a flow with a continuous power spectrum. An aspect of the Taylor–Couette flow observations related to the Ruelle–Takens–Newhouse theory is the number of independent frequencies present in quasiperiodic flows. Gorman *et al.*[5] observed quasiperiodic flows, with three independent frequencies in Taylor–Couette flow. Gollub and Benson[1] identified different routes to turbulence in Rayleigh–Bénard convective flows, depending on the aspect ratio, Prandtl number, and mean flow. They found flows with broad spectra preceded in Rayleigh number by quasiperiodic flows with two or three frequencies, as well as a succession of subharmonic, periodic-doubling bifurcations preceding the onset of broad spectra. Walden *et al.*[12] observed quasiperiodic flows in Rayleigh–Bénard convection with four and five independent frequencies.

The process that leads a predictable flow to an unpredictable, but deterministic, chaotic regime has also been studied by numerical approaches. Numerical simulations have been successfully performed in closed and open flow such as Rayleigh–Bénard convection, plane, and modified channel flows.[3,13–16] McLaughlin and Orszag[3] found periodic, quasiperiodic, and chaotic behavior in their transitional study on thermal convection. Their results appear to be consistent with the Ruelle–Takens–Newhouse theory, in that simulated flows with three or more distinct frequencies also contain broadband frequency spectrum. Ghaddar *et al.*[15] have made a thorough study of flows in grooved channels by means of two-dimensional simulations using spectral domain-decomposition methods. They determined that nonlinear ef-

 1070-6631/94/6(6)/1994/9 © 1994 American Institute of Physics

fects lead to self-sustained oscillatory flows beyond the critical Reynolds number. Amon and Patera[16] performed three-dimensional investigations on these grooved-channel flows, and found that the self-sustained oscillations admit a secondary instability. The flow in the grooved channel undergoes a supercritical regular Hopf bifurcation at a Reynolds number that is dramatically lower than the corresponding value for plane Poiseuille flow. For some range of Reynolds numbers, the secondary instability saturates in a steady-periodic three-dimensional, low-order equilibrium.[16] This three-dimensional equilibrium owes its stability and existence to the narrow band nature of the grooved-channel-flow secondary instability.

Blondeaux and Vittori[17] numerically studied the transition process, which leads the oscillatory flow over a wavy wall from a periodic behavior to chaos by a Feigenbaum scenario. They found that by increasing the Reynolds number, the flow experiences an infinite sequence of period doubling (pitchfork bifurcations), which takes place at successive critical values. A chaotic behavior is obtained both for a fixed geometrical configuration, increasing the Reynolds number, and for fixed characteristics of the oscillatory flow, increasing the amplitude of the wall waviness. In both cases the flow experiences an infinite sequence of period doubling, either in a finite interval of the Reynolds number or in a finite range of the waviness height. Schatz *et al.*[18] demonstrated, by a laboratory experiment and numerical simulations on a spatially perturbed plane channel, that the primary instability to stable two-dimensional traveling waves occurs as a supercritical Hopf bifurcation. They also presented evidence from laboratory experiments for a secondary transition leading to a stable-ordered state in the open flow through a spatially perturbed plane channel.[19] Their results suggest that open flows can exhibit a sequence of bifurcations to stable nonturbulent states. Batcho and Karniadakis[20] found that successive supercritical states are established through a series of period doubling before a chaotic state is reached in flows past a heated cylinder.

Numerical calculations and experimental studies have been performed in converging–diverging channels,[21–26] and global flow patterns have been reported. These flows are characterized by a zone of separation for low Reynolds numbers, a vortex regime with a recirculation zone for larger Reynolds numbers, and a mixing region with the mainstream. These previous studies have only considered periodic, fully developed steady flows and pulsating external flows. However, the basic mechanisms of unsteady oscillatory motion, the transition process and the route to chaos have not been previously reported for open flows in converging–diverging channels.

In this paper we investigate the transition and onset of chaos in converging–diverging channel flows by direct numerical simulation using the spectral element method. Our results indicate that the flow experiences a sequence of instabilities, reaching a chaotic regime after a finite number of supercritical Hopf bifurcations. A transition process similar to that described by the Ruelle–Takens–Newhouse theory is reported for the first time in forced convective open system flows.

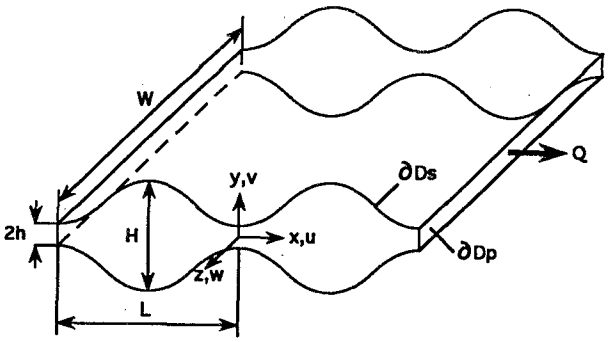

FIG. 1. Symmetric converging–diverging channel: nondimensionalized periodicity length $L/h=9.33$, spanwise length $W/h=53.33$, and maximum height $H/h=6.66$.

In Sec. II we present the problem formulation. In Sec. III we introduce the numerical procedure for the temporal and spatial discretization. In Sec. IV we report results of the numerical simulations in terms of time-velocity histories, Fourier power spectra, and phase space trajectories, for increasing Reynolds numbers from subcritical to supercritical flow regimes. In Sec. V we summarize the results and discuss the Ruelle–Takens–Newhouse scenario to chaos. Last, in Sec. VI we present the conclusions of this work.

II. PROBLEM FORMULATION

We consider unsteady, incompressible flow in the periodically converging–diverging channel with sinusoidal walls, as shown in Fig. 1. The flow is assumed to be fully developed in the streamwise direction x and homogeneous in the spanwise direction z. The governing equations are the Navier–Stokes, and continuity equations, given by

$$\frac{\partial \mathbf{v}}{\partial t} = \mathbf{v}\times\boldsymbol{\omega} - \nabla\Pi + \mathrm{Re}^{-1}\,\nabla^2\mathbf{v}, \quad \text{in } D, \tag{1}$$

$$\nabla\cdot\mathbf{v}=0, \quad \text{in } D, \tag{2}$$

where the computational domain D is defined by the periodicity length between furrows, L. Here, $\mathbf{v}(\mathbf{x},t)=U\hat{i}+V\hat{j}+W\hat{k}$ is the velocity; $\mathbf{x}$ and t represents space and time, respectively; $\Pi=p+(\frac{1}{2})\mathbf{v}\cdot\mathbf{v}$ is the dynamic pressure; $\boldsymbol{\omega}=\nabla\times\mathbf{v}$ is the vorticity, and $\mathrm{Re}=(\frac{3}{2})Vh/\nu$ is the Reynolds number, where ν is the kinematic viscosity of the fluid and V is the time-mean cross-channel average velocity. All variables considered are nondimensionalized by the centerline velocity $(\frac{3}{2})V$, half-height of the channel $h/2$, and convective time.

The fully developed boundary conditions for the velocity $\mathbf{v}(\mathbf{x},t)$ are

$$\mathbf{v}(\mathbf{x},t)=0, \quad \text{on } \partial D_s, \tag{3}$$

$$\mathbf{v}(x+nL,y,z,t)=\mathbf{v}(x,y,z,t), \quad \text{on } \partial D_p, \tag{4}$$

corresponding to no slip on the rigid walls ∂D_s and periodicity on ∂D_p of the fully developed flow in the x direction; n is an integer periodicity index whose value for the simulations reported is unity. For the pressure, we require

$$\Pi(\mathbf{x},t)=-f(t)x+\tilde{\Pi}(\mathbf{x},t), \tag{5}$$

$$\tilde{\Pi}(x+nL,y,z,t)=\tilde{\Pi}(x,y,z,t), \tag{6}$$

TABLE I. Fundamental frequencies for different Reynolds numbers Re and mesh resolutions. Here S and C denote the number of macroelements in the streamwise and crosswise directions, respectively, and N^2 is the number of nodes per macroelement.

Mesh		Re=150		Re=400			
Macroelements $S\times C$	Nodes per macroelement N^2	ω_1 (error %)		ω_1 (error %)		ω_2 (error %)	
8×4	49	0.321 651 1	(−1.80)	0.290 888 0	(−3.52)	0.436 332 0	(0.18)
8×4	81	0.318 396 9	(−2.79)	0.290 881 1	(−3.52)	0.440 252 5	(1.09)
16×4	49	0.329 840 4	(0.69)	0.309 683 5	(2.69)	0.434 748 0	(−0.17)
32×4	49	0.329 852 2	(0.70)	0.310 885 7	(3.11)	0.439 528 0	(0.92)
16×8	81	0.325 594 0		0.301 503 5		0.435 505 0	

where the driving pressure gradient $f(t)$ is determined by imposing the flow rate condition,

$$Q=\int_{-h}^{h} u(x=0,y,z,t)dy=\frac{4}{3}. \tag{7}$$

The linear pressure term in Eq. (5) is consistent with periodicity of the velocity [Eq. (4)] since only the gradient of the pressure enters in Eq. (1).

III. NUMERICAL APPROACH

The numerical results are obtained by direct simulation of the time-dependent Navier–Stokes equations integrating in time, starting with a predicted steady flow and gradually increasing the Reynolds number until a steady, time-periodic, or transitional state is found. Increases in Reynolds numbers are made in relatively small steps, so that the dynamic flow evolution can be followed in detail. The initial conditions for subsequent simulations are those associated with the preceding lower Reynolds number. However, to investigate the possibility of hysteresis effects, several cases were simulated using different initial conditions corresponding to flow fields at both lower and higher Reynolds numbers. These simulations yielded the same time-asymptotic evolution of the flow pattern. This verifies that the solutions are independent on the initial conditions for Reynolds numbers up to 600. Simulations are performed for an integration time long enough to yield statistically stationary frequencies to within 0.5%. This requires about 10^5 time steps for a Reynolds number of 400.

A. Temporal and spatial discretization

The governing equations [(1) and (2)], subject to the boundary conditions [(3) and (4)], are solved numerically using a spectral element method.[27,28] A three-step, time-splitting scheme for the semidiscrete formulation of the time-dependent term in the Navier–Stokes equations is employed. This time-stepping procedure consists of a first nonlinear step for the convective term using an explicit third-order, forward-in-time Adams–Bashforth scheme; a second pressure step using an implicit Euler-backward scheme for the pressure term and enforcing the incompressibility constraint; and, finally, a third viscous step employing an implicit Crank–Nicolson scheme, which includes the viscous corrections and imposes the boundary conditions. A complete description of this time-splitting scheme is given in Refs. 13 and 27.

For the spatial discretization in this spectral element method, the domain is first divided into quadrilateral macroelements, which are isoparametrically mapped from the physical space $\mathbf{x}=\mathbf{x}(x,y,z)$ into the local coordinate system $\mathbf{s}=\mathbf{s}(p,q,r)$. Then the geometry, velocity, and pressure in each macroelement is represented as a tensor product of high-order Lagrangian interpolants through Gauss–Lobatto–Chebyshev collocation points, defined as

$$(\mathbf{x},\mathbf{v},\Pi)_n^l(\mathbf{s})=\sum_{i=0}^{N}\sum_{j=0}^{N}\sum_{k=0}^{N}(\mathbf{x},\mathbf{v},\Pi)_{ijk}^l h_i(p)h_j(q)h_k(r), \tag{8}$$

where $h_i(p)$, $h_j(q)$, and $h_k(r)$ are Nth-order Lagrangian interpolants (truncated series of Chebyshev polynomials) that satisfy $h_i(\xi jk)=\delta_{ijk}$ at the local (p,q,r) coordinates. The nonlinear convective term is evaluated pseudospectrally, whereas the pressure and viscous terms, which correspond to modified Helmholtz equations, are solved by a variational approach.[28]

This nondiffusive numerical methodology is well suited to investigate temporal transition in self-sustained oscillatory flows, since high-frequency flow oscillations are not damped by artificial numerical viscosity. Moreover, the predicted flows correspond to stable solutions that are physically realizable, as they are the result of evolution, not equilibrium, calculations.

B. Mesh refinement studies

The computations were performed with different mesh resolutions to investigate the adequacy of the spatial discretization as the governing parameter, Re, is increased. Table I summarizes the results for five meshes that differ in the number of macroelements as well as in the order of Chebyshev interpolants. This mesh refinement study shows that the first fundamental frequency, ω_1, calculated with the coarser mesh, differs from a mesh-independent result by a maximum of 3.5%, in the range of Reynolds numbers investigated. As a compromise between computing resources and accuracy, the 8×4×49 mesh is used for all the computations reported in this paper, unless otherwise stated. A typical computational spectral element mesh is shown in Fig. 2.

IV. RESULTS

We now present numerical results of two-dimensional flow simulations in the converging–diverging channel. The

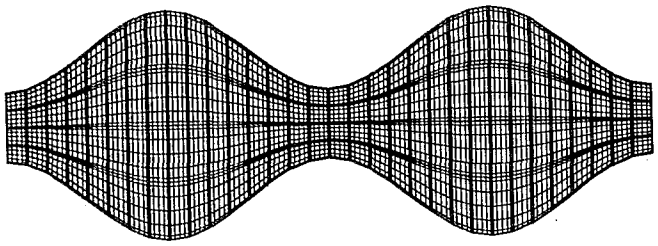

FIG. 2. Computational domain and spectral element mesh.

flow evolution corresponds to successive supercritical Hopf bifurcations obtained by increasing the Reynolds number and depicted in terms of time–velocity histories, power spectra, and phase space trajectories to identify periodic, quasiperiodic, and chaotic regimes. The $U(t)$ and $V(t)$ velocities time series, the Fourier power spectra, and the phase space trajectories shown in this paper correspond to a point located at the central line of the channel $[(x,y,z)=(L/2,0,w/2)$ in Fig. 1].

A. Transition to unsteady flow

For Reynolds number lower than 20, the flow streamlines the sinusoidal walls of the channel without reversing its direction. This is in good agreement with the experimental results reported by Nishimura *et al.*[26] in this geometry with same aspect ratios. Figure 3 shows a time-asymptotic result for the streamwise U velocity converging to its steady state at Re=125. We observe that the least-stable mode is oscillatory, with an exponential decay rate $\sigma=-0.000\,462$ and angular frequency $\omega=0.313\,490$, where the frequency is nondimensionalized by the convective time. Notice that the decay rate and frequency of the least-stable Tollmien–Schlichting (TS) mode for a plane channel flow of wave number, $\alpha=2\pi m/(L/h)^*=0.738\,069$ is $\sigma_{TS}=-0.139\,409$ and $\omega_{TS}=0.313\,475$, where m is the number of waves per periodicity and $(L/h)^*=8.513$. The frequency of the sinusoidal channel decay mode, which is close to the frequency

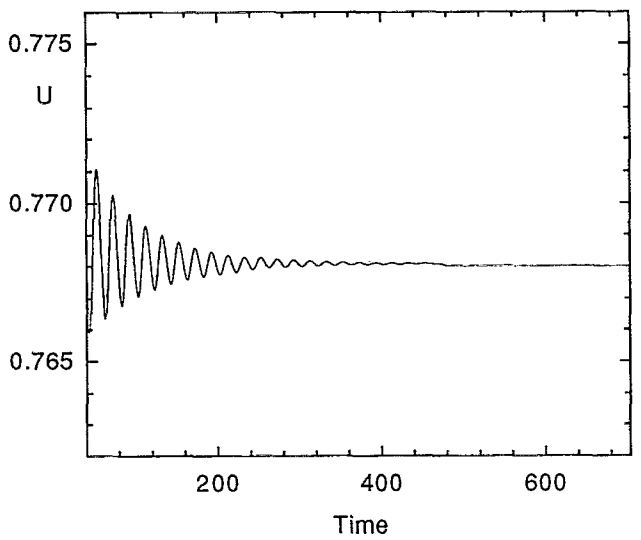

FIG. 3. Streamwise U velocity as a function of time at Re=125.

of a plane channel mode with the same wave spatial structure, verifies that the instabilities are Tollmien–Schlichting in nature, while the decay rate indicates the destabilizing effect of the sinusoidal walls.

The flow in this converging–diverging channel first becomes unstable and bifurcates to a periodic solution at a critical Reynolds number between 130 and 135. For slightly supercritical Reynolds numbers, a harmonic regime develops, where the flow oscillates with a fundamental frequency ω_1. Traveling waves are observed inducing self-sustained oscillatory flows that become more complex with larger amplitudes and smaller frequencies as the Reynolds number is increased. For larger supercritical Reynolds numbers, the flow evolves gradually from a periodic behavior to chaos via supercritical Hopf bifurcations. The investigation of the flow evolution enables us to establish the route of transition, and the knowledge of the combination the frequencies generated allow us to determine the evolutive pattern for the origin of chaos in converging–diverging channel flows.

B. Periodic, quasiperiodic, and chaotic flow regimes

Figure 4 depicts the sequence of transitions that are observed reversibly as the Reynolds number is varied between Re=150 and Re=750. Figure 4(a) shows the periodic behavior for Re=150, indicating that the flow has bifurcated to a limit cycle or periodic attractor. The time evolution of the U (streamwise) and V (crosswise) velocities for this Reynolds number represents a sinusoidal function corresponding to the self-sustained oscillatory flow. These signals have evolved, starting from a steady state to a periodic regime by a first bifurcation of the flow. The growth of the instabilities is saturated by nonlinearities and the flow settles into a time-periodic, self-sustained oscillatory flow with one fundamental frequency, $\omega_1=0.321\,651$, as it is shown by the Fourier power spectrum of the U velocity. The logarithmic power spectrum contains three strong peaks at the frequency ω_1 and its harmonics $2\omega_1$ and $3\omega_1$. The foregoing motion can also be described by its trajectory in a suitable phase space.[29] The phase space trajectory of the V vs U velocities approaches a limit cycle. The ratio of the fundamental frequencies associated with the x- and y-flow directions is given by $\omega_x/\omega_y=2$ at centerline points located symmetrically in the channel. Other points of the flow field exhibit a frequency ratio $\omega_x/\omega_y=1$. The stable nature of the periodic solution with respect to perturbations is strongly dependent on nonlinear flow effects, which allow the solution to change gradually from a laminar steady state to a time-periodic regime.

As the Reynolds number is increased, a second time-dependent instability occurs and a new characteristic frequency, ω_2, appears. Figure 4(b) shows the time evolution of the U and V velocities at Re=200, which represents a quasiperiodic flow regime with two characteristic fundamental frequencies and their linear combinations. The ratio ω_1/ω_2 is an irrational number, as indicated in the corresponding Fourier power spectrum [Fig. 4(b)]. The phase space trajectory also depicts the quasiperiodic behavior, where the solution has experienced a permanent translational motion around the periodic solution obtained for Re=150.

Similar quasiperiodic behaviors are obtained for Reynolds numbers 250, 300, and 350, as shown in Figs. 4(c)–4(e). In all these cases, both fundamental frequencies are incommensurate and close to those obtained for Re=200. The first fundamental frequency, ω_1, closely matches the least-stable Tollmien–Schlichting frequency for plane channel flow. The subharmonics and superharmonics in the power spectra are linear combinations of the fundamental frequencies related by $(m_1\omega_1+m_2\omega_2)$, with m_1 and m_2 integers. The ratios ω_1/ω_2 decrease and the velocity amplitudes increase in these quasiperiodic flows as the Reynolds number is increased. The phase space trajectories indicate that the flow solution experiences a continuous translation around the periodic solution at Re=150, and the mirror pattern of the

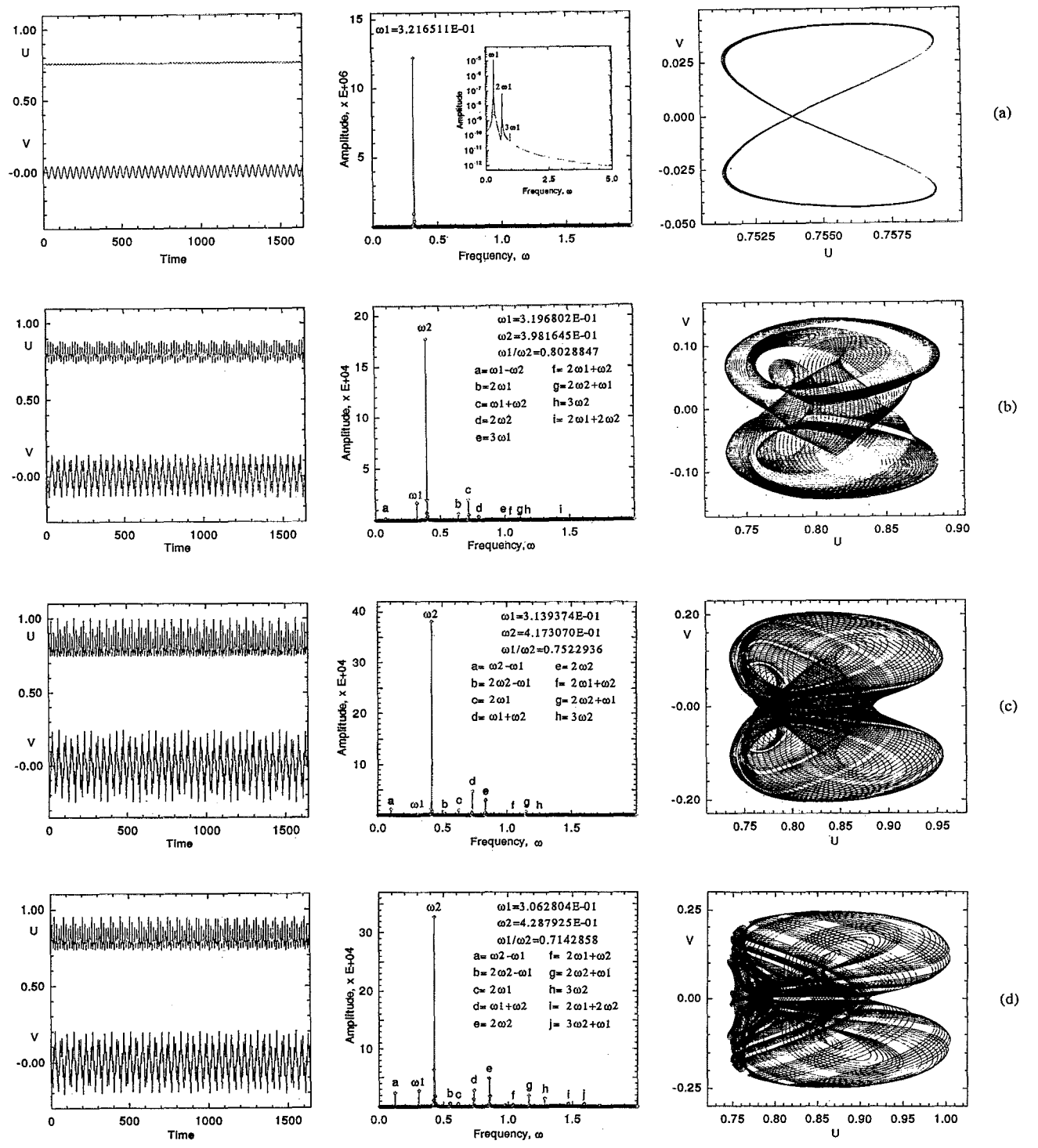

FIG. 4. Streamwise U and crosswise V velocities as a function of time, Fourier power spectra of the U velocity, and phase space trajectories of V vs U for the converging–diverging channel flow: (a) Re=150; (b) Re=200; (c) Re=250; (d) Re=300; (e) Re=350; (f) Re=400; (g) Re=500; and (h) Re=750.

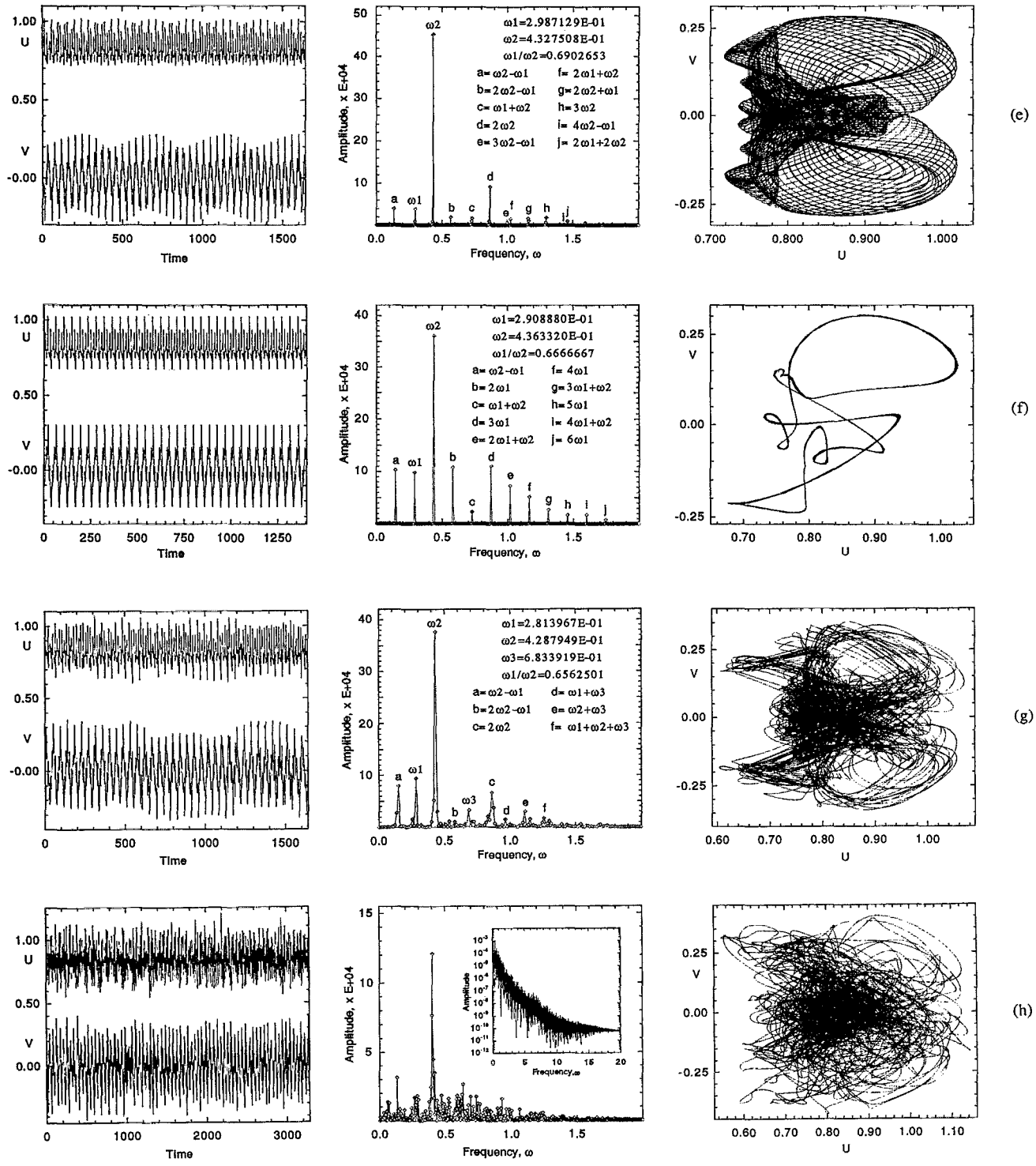

FIG. 4. (*Continued.*)

trajectories with respect to $V=0$ tends to disappear at these Reynolds numbers.

The complexity of the system dynamics is affected by a frequency-locking phenomenon as the Reynolds number is further increased. This is shown for Re=400, where the velocity histories, phase space trajectory, and power spectrum all have a more regular appearance [Fig. 4(f)]. In fact, the closed phase space trajectory indicates that the periodic behavior has been restored, and the power spectrum has regularly occurring peaks corresponding to pure harmonics of

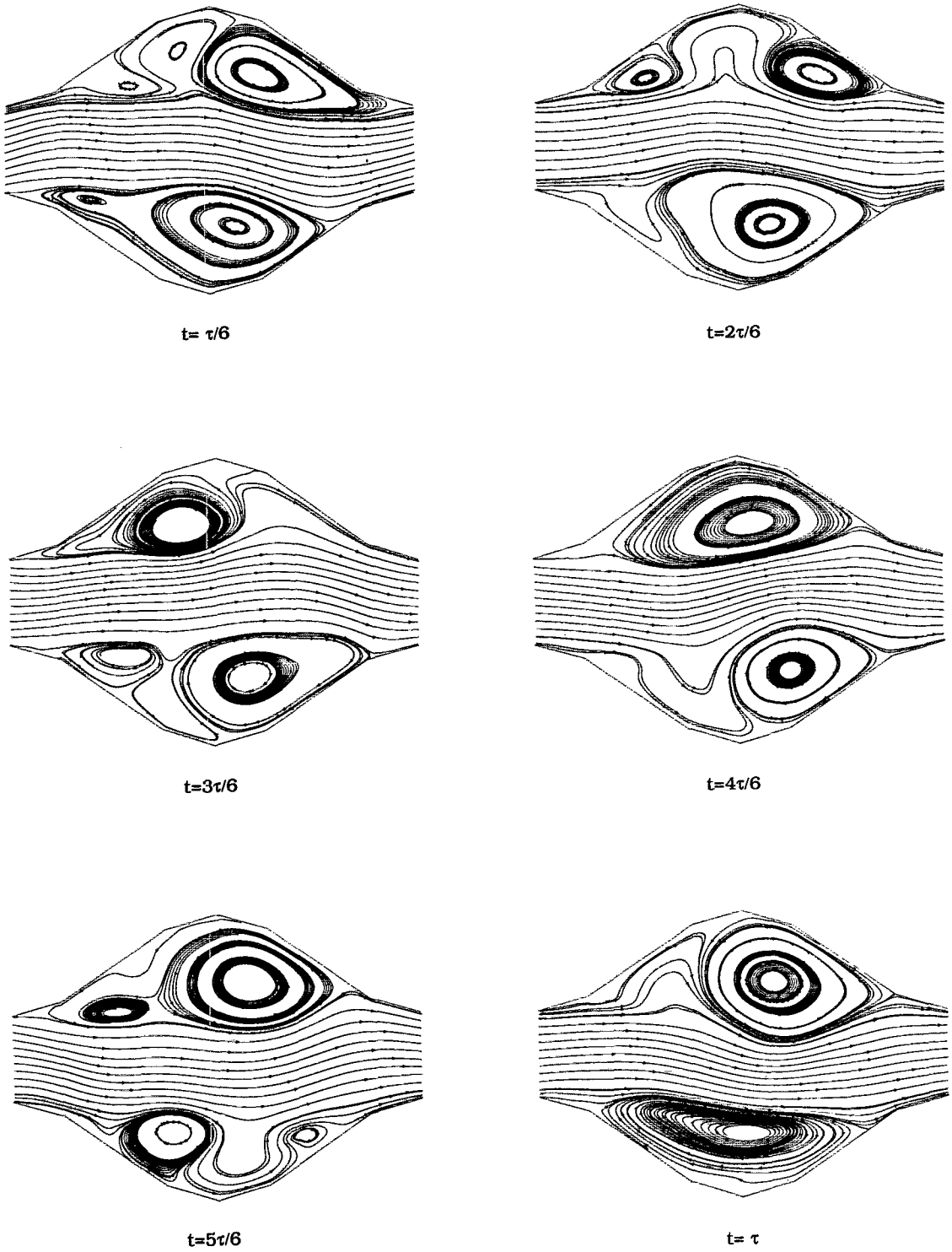

FIG. 5. Instantaneous streamlines plot in a sequence of six time frames within one flow cycle ($0 \leq t \leq \tau$) at Re=400.

($\omega_2 - \omega_1$). This is due to the synchronization of the two oscillators in the system and the frequency-locking—a phenomenon that has also been found in other dynamical systems.[29] The distance between any two consecutive harmonics is given by $2\pi/\tau$, with a nondimensional period $\tau = 43.04$. The phase space trajectory of V vs U for 32 complete periods of oscillations τ shows that the velocity trajectories are moving along a limit cycle and periodic attractor, corresponding to its frequency-locked periodic solution. The mirror pattern for the trajectories observed at lower Reynolds numbers is not obtained in this flow regime, and the ratio between the frequencies associated to the x and y directions of the flow is $\omega_x/\omega_y = 1$.

In Fig. 5, the global flow structure is shown through a sequence of six time frames of the instantaneous streamlines during one period of self-sustained oscillatory flow at Re

=400. The traveling wave structure of this supercritical flow confirms that the flow has undergone a bifurcation from a steady, time-independent state to a time-periodic flow. The viscous forces are not strong enough to keep the vortices confined in the sinusoidal furrows of the converging–diverging channel. These vortices are moving alternately in the upper and lower furrow, inducing mixing with the bulk flow. The wave crest travels a periodicity length L while two vortices are ejected from the furrows during one period of oscillation τ. Therefore, the vortex dynamics are synchronized with the traveling wave structure of the flow.

When we compute the flow at Re=500 [Fig. 4(g)], the asymptotically converged time signals of the velocity components and their Fourier power spectra show that the flow has undergone another bifurcation. This bifurcation leads to a quasiperiodic behavior and attractor, with three fundamental frequencies, ω_1, ω_2, and ω_3, and their linear combinations. We notice that the first two frequencies, ω_1 and ω_2, are close to those obtained for previous flow regimes. According to Eckmann,[30] when a system undergoes three Hopf bifurcations starting from a stationary solution as a parameter is varied (e.g., the Reynolds number), then it is likely that the system possesses a strange attractor with sensitivity to initial conditions after the third bifurcation. The power spectrum of such a system will exhibit one, then two, and possibly three independent fundamental frequencies. When the third frequency is about to appear, a broadband spectrum will appear simultaneously if there is a strange attractor. This can be interpreted as chaotic evolution of the system.

As the Reynolds number is further increased, an aperiodic behavior, associated with a strange attractor, is observed for Re=750, where the time evolution of the velocity components clearly depicts its chaotic behavior [Fig. 4(h)]. The Fourier power spectrum shows that the sharp peaks at the previous fundamental frequencies decrease in amplitude and tend to disappear in the background of a broadband continuous spectrum. However, there are still prevailing frequencies, ω_1, ω_2, and ω_3, on the continuous spectrum, where ω_1 corresponds to the least-stable Tollmien–Schlichting mode. According to Ruelle's theory, this evolution is governed by a strange attractor, since a continuous frequency spectrum solution comes after a quasiperiodic behavior insensitive to initial conditions.[31]

V. DISCUSSION: RUELLE–TAKENS–NEWHOUSE SCENARIO

The results presented in previous sections indicate that the converging–diverging channel flow experiences three successive supercritical Hopf bifurcations from a laminar steady state to an aperiodic flow regime, and each bifurcation adds a new fundamental frequency. In addition, there are intermediate states of periodicity with one fundamental frequency, quasiperiodicity with two incommensurate fundamental frequencies, frequency-locked periodicity, and quasiperiodicity with three fundamental frequencies along with linear combinations of these frequencies.

The first fundamental frequency of the oscillatory flow, ω_1, is related to the traveling Tollmien–Schlichting wave frequency associated with the least-stable channel mode for all Reynolds numbers investigated. To obtain the least-stable plane channel mode compatible with the converging–diverging channel, we calculate the Tollmien–Schlichting frequency, ω_{TS}, for a plane channel, solving the Orr–Sommerfeld equation.[32] Table II compares ω_{TS} with ω_{FS} as a function of the Reynolds number, where ω_{FS} is the fundamental frequency for the converging–diverging channel flow obtained from the Fourier spectrum analysis of the direct numerical simulations. In the vicinity of the first flow bifurcation, there is very good agreement between the first fundamental frequency of the converging–diverging channel flow, and the Tollmien–Schlichting frequency predicted by linear stability analysis. Near this first bifurcation, the flow either decays toward a steady state or oscillates with infinitesimally small amplitudes. This suggests that the amplified instabilities are Tollmien–Schlichting in nature. However, for strongly supercritical flows, the large-amplitude oscillations exhibit a fundamental frequency shifted from ω_{TS}. This is due to nonlinear effects that are significant for finite-amplitude oscillations. Therefore, the traveling wave structure and the characteristics for small-amplitude instabilities support the assertion that the converging–diverging channel instabilities are triggered by Tollmien–Schlichting instabilities.

TABLE II. Tollmien–Schlichting (ω_{TS}) and Fourier spectrum frequencies (ω_{FS}) for different Reynolds numbers.

		ω_{FS}		
Re	ω_{TS}	First	Second	Third
125	0.313 475	0.313 490		
140	0.306 207	0.321 651		
150	0.302 015	0.321 651		
200	0.284 748	0.319 680	0.398 164	
250	0.273 059	0.313 937	0.417 307	
300	0.264 214	0.306 280	0.428 792	
350	0.256 918	0.298 712	0.432 750	
400	0.250 880	0.290 888	0.436 332	
500	0.241 522	0.281 396	0.428 794	0.683 391

In summary, the converging–diverging channel flow follows a route to chaos with successive supercritical Hopf bifurcations as the Reynolds number is increased. This transition scenario, reported here for the first time in open flow systems, is similar to the Ruelle–Takens–Newhouse scenario to chaos in dissipative dynamical systems,[7] which has been found in closed flow systems such as Taylor–Couette flow[4,5] and in Rayleigh–Bénard thermal convection.[1,3,12] The pres-

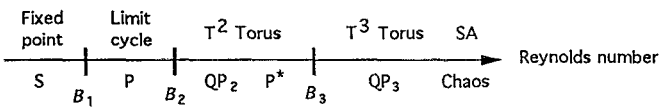

FIG. 6. Schematic representation of the successive bifurcations B_1, B_2, and B_3 leading to chaos as the Reynolds number is increased: S=steady state; P=periodic state; QP_2=quasiperiodic regime with two incommensurate fundamental frequencies; P*=frequency-locked periodic state; QP_3 =quasiperiodic regime with three incommensurate fundamental frequencies; SA=strange attractor.

ence of the third fundamental frequency at the onset of chaos and the chaotic behavior observed for the higher Reynolds number (750), suggests the existence of a strange attractor. The following states and bifurcations are identified for the evolution of the forced convective flow in converging–diverging channels, as shown in Fig. 6: (i) *laminar steady-state flow*; first bifurcation, B_1; (ii) *periodic flow* with one fundamental frequency; second bifurcation, B_2; (iii) *quasi-periodic flow* with two incommensurate fundamental frequencies and their linear combinations; (iv) *frequency-locked periodic state;* third bifurcation, B_3; (v) *quasiperiodic flow* with three incommensurate fundamental frequencies and their linear combinations; and (vi) *aperiodic chaotic state.*

VI. CONCLUSION

Self-sustained oscillatory flows are investigated by the direct numerical simulation of incompressible flows in converging–diverging channels. The numerical results reveal that the transition process from laminar to chaotic flow follows a scenario similar to that described by the Ruelle–Takens–Newhouse theory, characterized by a finite number of successive supercritical Hopf bifurcations. These flows exhibit a sequence of periodic, quasiperiodic, and aperiodic regimes, as the Reynolds number is increased beyond the first flow bifurcation at $130<\mathrm{Re}<135$. Quasiperiodic flow regimes with two and three incommensurate fundamental frequencies, as well as a frequency-locked periodic regime, are also obtained as intermediate states. Previous to the onset of the chaotic flow regime, the velocity power spectrum contains three fundamental frequencies along with their linear combinations. An aperiodic behavior, associated with a strange attractor, is observed for $\mathrm{Re}=750$. The chaotic behavior for this regime is indicated by a broadband Fourier power spectrum. The first fundamental frequency for all Reynolds numbers is related to the least-stable channel mode and corresponds to the traveling Tollmien–Schlichting wave mode.

ACKNOWLEDGMENTS

We gratefully acknowledge the support of this work by the Chilean MIDEPLAN Scholarship (A.M.G.) and by the National Science Foundation Grant Nos. INT-9123807 and CTS-9311072.

[1]J. P. Gollub and S. H. Benson, "Many routes to turbulent convection," J. Fluid Mech. **100**, 449 (1980).
[2]M. Giglio, S. Musazzi, and U. Perini, "Transition to chaotic behavior via a reproductible sequence of period-doubling bifurcations," Phys. Rev. Lett. **47**, 243 (1981).
[3]J. B. McLaughlin and S. A. Orszag, "Transition from periodic to chaotic thermal convection," J. Fluid Mech. **122**, 123 (1982).
[4]J. P. Gollub and H. L. Swinney, "Onset of turbulence in a rotating fluid," Phys. Rev. Lett. **35**, 927 (1975).
[5]M. Gorman, L. A. Reith, and H. L. Swinney, "Modulation patterns, multiple frequencies, and other phenomena in circular Couette flow," Ann. NY Acad. Sci. **357**, 10 (1980).
[6]D. Ruelle and F. Takens, "On the nature of turbulence," Commun. Math. Phys. **20**, 167 (1971).
[7]S. Newhouse, D. Ruelle, and F. Takens, "Occurrence of strange axiom A attractors near quasiperiodic flow on T^m, $m\geqslant 3$," Commun. Math. Phys. **64**, 35 (1978).
[8]M. Feigenbaum, "The transition to aperiodic behavior in turbulent systems," Commun. Math. Phys. **77**, 65 (1980).
[9]P. Manneville and Y. Pomeau, "Different ways to turbulence in dissipative dynamical systems," Physica D **1**, 219 (1980).
[10]J. Guckenheimer, "Strange attractors in fluids: Another view," Annu. Rev. Fluid Mech. **18**, 15 (1986).
[11]F. C. Moon, *Chaotic and Fractal Dynamics. An Introduction for Applied Scientists and Engineers* (Wiley, New York, 1992).
[12]R. W. Walden, P. Kolodner, A. Passner, and C. M. Surko, "Nonchaotic Rayleigh–Benard convection with four and five incommensurate frequencies," Phys. Rev. Lett. **53**, 242 (1984).
[13]S. A. Orszag and L. C. Kells, "Transition to turbulence in plane Poiseuille flow and plane Couette flow," J. Fluid Mech. **96**, 159 (1980).
[14]S. A. Orszag and A. T. Patera, "Secondary instability of wall-bounded shear flows," J. Fluid Mech. **128**, 347 (1983).
[15]N. K. Ghaddar, K. Z. Korczak, B. B. Mikic, and A. T. Patera, "Numerical investigation of incompressible flow in grooved channels. Part 1. Stability and self-sustained oscillations," J. Fluid Mech. **163**, 99 (1986).
[16]C. H. Amon and A. T. Patera, "Numerical calculation of stable three-dimensional tertiary states in grooved-channel flow," Phys. Fluids A **1**, 2005 (1989).
[17]P. Blondeaux and G. Vittori, "A route to chaos in an oscillatory flow: Feigenbaum scenario," Phys. Fluids A **3**, 2492 (1991).
[18]M. F. Schatz, R. P. Tagg, H. L. Swinney, P. F. Fischer, and A. T. Patera, "Supercritical transition in plane channel flow with spatially periodic perturbations," Phys. Rev. Lett. **66**, 1579 (1991).
[19]M. F. Schatz and H. L. Swinney, "Secondary instability in plane channel flow with spatially periodic perturbations," Phys. Rev. Lett. **69**, 434 (1992).
[20]P. Batcho and G. E. Karniadakis, "Chaotic transport in two- and three-dimensional flow past a cylinder," Phys. Fluids A **3**, 1051 (1991).
[21]I. J. Sobey, "On flow through furrowed channels. Part 1. Calculated flow patterns," J. Fluid Mech. **96**, 1 (1980).
[22]I. J. Sobey, "Oscillatory flow at intermediate Strouhal number in asymmetric channels," J. Fluid Mech. **125**, 359 (1982).
[23]E. M. Sparrow and A. T. Prata, "Numerical solutions for laminar flow and heat transfer in a periodically converging–diverging tube with experimental confirmation," Numer. Heat Transfer **6**, 441 (1983).
[24]M. Faghri and Y. Asako, "Numerical determination of heat transfer and pressure drop characteristics for a converging–diverging flow channel," ASME J. Heat Transfer **109**, 606 (1987).
[25]T. Nishimura, Y. Ohosi, and Y. Kawamura, "Flow characteristics in a channel with symmetric wavy wall for steady flow," J. Chem. Eng. Jpn. **17**, 466 (1984).
[26]T. Nishimura, S. Murakami, S. Arakawa, and Y. Kawamura, "Flow observations and mass transfer characteristics in symmetrical wavy-walled channels at moderate Reynolds number for steady flow," Int. J. Heat Mass Transfer **33**, 835 (1990).
[27]C. H. Amon, "Spectral element-Fourier method for transitional flows in complex geometries," AIAA J. **31**, 42 (1993).
[28]A. T. Patera, "A spectral element method for fluid dynamics: Laminar flow in a channel expansion," J. Comput. Phys. **54**, 468 (1984).
[29]P. Berge, Y. Pomeau, and C. Vidal, *Order Within Chaos* (Wiley, New York, 1986).
[30]J. P. Eckmann, "Roads to turbulence in dissipative dynamical systems," Rev. Mod. Phys. **53**, 643 (1981).
[31]D. Ruelle, "Strange attractors," Math. Intell. **2**, 126 (1980).
[32]P. G. Drazin and W. H. Reid, *Hydrodynamic Stability* (Cambridge University Press, Cambridge, 1981).